A98-31523

ICAS-98-2,9,2

AERODYNAMIC DESIGN OF HIGH-PERFORMANCE SAILPLANE WING-FUSELAGE COMBINATIONS

L.M.M. Boermans
Delft University of Technology
Faculty of Aerospace Engineering
Kluyverweg 1, 2629 HS Delft, The Netherlands

F. Nicolosi
University of Naples "Federico II"
Department of Aeronautical Engineering
Via Claudio 21, 80125 Naples, Italy

K. Kubrynski
Technical University of Warshaw
Institute of Applied Mechanics and Aviation
ul. Nowawiejska 22/24, Warshaw, Poland

Abstract

The paper deals with the design of high-performance sailplane fuselages and wing-fuselage combinations.
The first part of the paper presents computational results of the effect of some fuselage design parameters on drag.
The second part of the paper describes the interference effects on wing-fuselage combinations and the way the negative effects were encountered in the design of two new combinations. One combination has a wing with camber changing flap, and the second one has a wing with spanwise camber. Each configuration employs modern laminar airfoils in its wing.
Flow visualization windtunnel tests substantiated the design objects. Prototypes of both configurations are being produced by German sailplane manufacturers.

Introduction

The aerodynamic quality of high-performance sailplanes has reached a high level; for instance the best glide ratio of 25m span sailplanes is about 60 which corresponds to a glide angle of about 1°. Wings, tailplanes and fuselages have been squeezed out for low drag, using advanced theoretical design methods in combination with windtunnel and free flight experiments[1-4]. When a wing and fuselage are combined, however, the flow in the junction is very complicated and not yet theoretically predictable with the required accuracy[5]. Hence, the design of a proper wing-fuselage junction has to be based on a judicious mixture of computational and experimental results, examples of which are shown in this paper.
In the next chapter the influence of some basic fuselage design parameters on fuselage drag has been evaluated theoretically. It is followed by a description of the interference effects on sailplane wing-fuselage configurations, and of the way the negative interference effects were encountered in the design of two new wing-fuselage configurations presented in the next chapters. The first configuration has a wing with camber changing flap, and the second configuration has a wing with spanwise camber.

Fuselage drag

In order to evaluate the effects of fuselage contraction, cockpit length, and height on fuselage drag, a three dimensional panel code coupled with a boundary layer integral method for axisymmetric bodies[6] was used. The e^n method in the approximate version[7] has been used to predict transition. The drag coefficient based on frontal area is computed by applying Young's formula[8] locally – yielding the equivalent drag distribution – and taking the maximum value at the tail.

Re=7.1e6	cd num.	cd exp.	xtr num.	xtr exp.
shape 1	0.0577	0.051	0.3	0.33
shape 2	0.0374	0.0338	0.35	0.35
shape 3	0.0392	0.0355	0.31	
shape 4	0.403	0.0379	0.29	0.31

Table 1 : Numerical/experimental drag coefficients and transition locations.

In Table 1 and Figures 1 and 2, transition positions and drag values obtained with the present method are compared with measured data[9] of 4 axisymmetric fuselages with different contractions. The calculated and measured data show the same trend; fuselage 2 has considerably less drag than fuselage 1, primarily due to

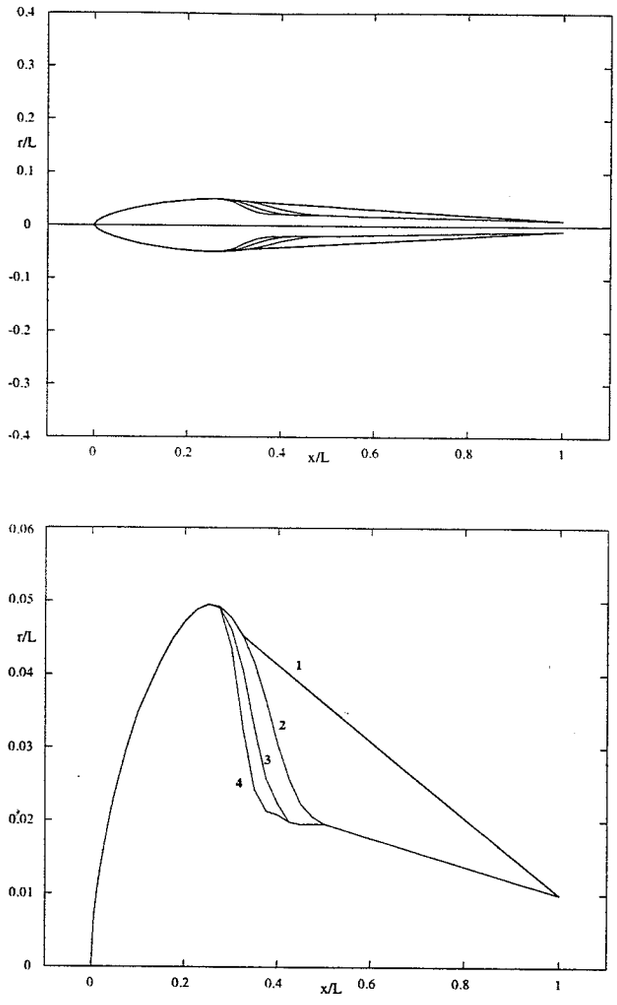

Figure1: Althaus axisymmetric bodies and radius distribution.

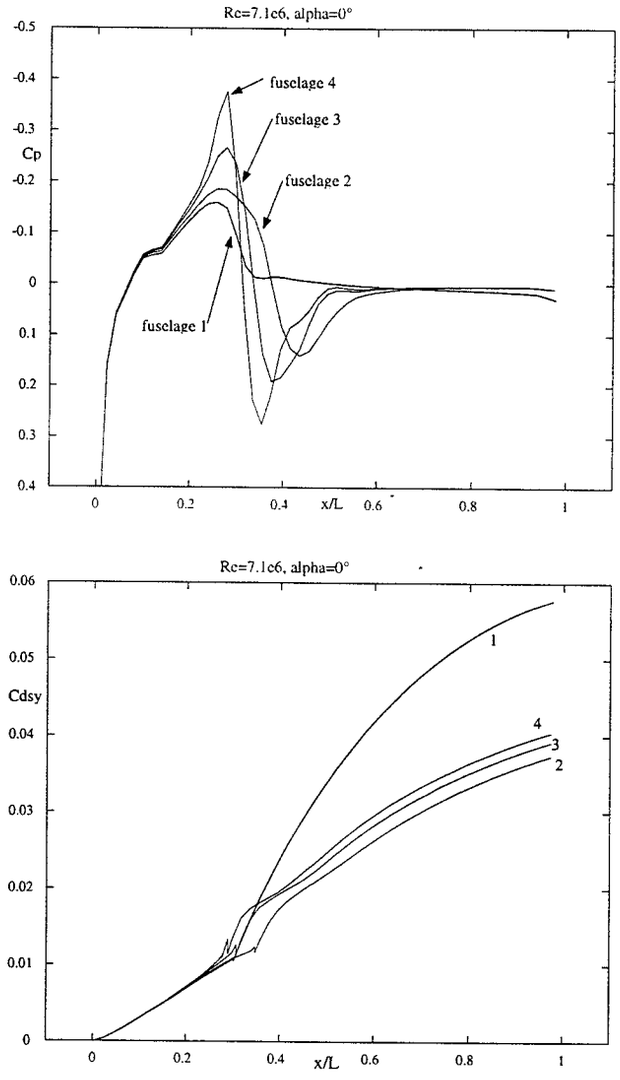

Figure 2: Pressure distributions, calculated transition positions, and equivalent drag distributions.

the reduced wetted surface. The higher contractions of fuselage 3 and 4 do not lead to a further drag reduction because contraction is applied such that the position of transition on these fuselages moves forward; as a result the drag accumulates to slightly higher value. If contraction is applied such that the position of transition does not change, calculations show that drag reduces with increase of contraction due to the decrease both in skin friction coefficient and in wetted surface behind the cockpit. Similarly, in case transition is fixed on the fuselage nose – to simulate the effect of rain or insects – the drag coefficient decreases with increasing contraction. When the contraction rate is too high however, the steep adverse pressure gradient causes the turbulent boundary layer to separate. This occurs on fuselage 4 of Figure 1, for instance.

Figure 3 shows results where the cockpit length of a fuselage is increased by 0.3m in order to create space for improved crashworthiness measures[10]: a longer survival cell and frontal absorbing structure. With transition at the same position, the larger laminar flow area but lower skin friction – due to the lower pressure gradient – yield the same drag coefficient.

In order to create space between the seat bottom and cockpit floor for crash absorbing elements[11], the height of the fuselage was increased by 10%. Figure 4 shows that the transition location is not influenced, but the increase in wetted area leads to a 13% higher drag coefficient.

The effects previously described are taken into account in the design of real fuselage shapes. Contraction on the top starts behind the pilot's head and underside contraction starts behind the pilot's seat. Adding the wing to the fuselage requires additional measures to be taken in order to reduce (interference) drag, as shown in the next chapters.

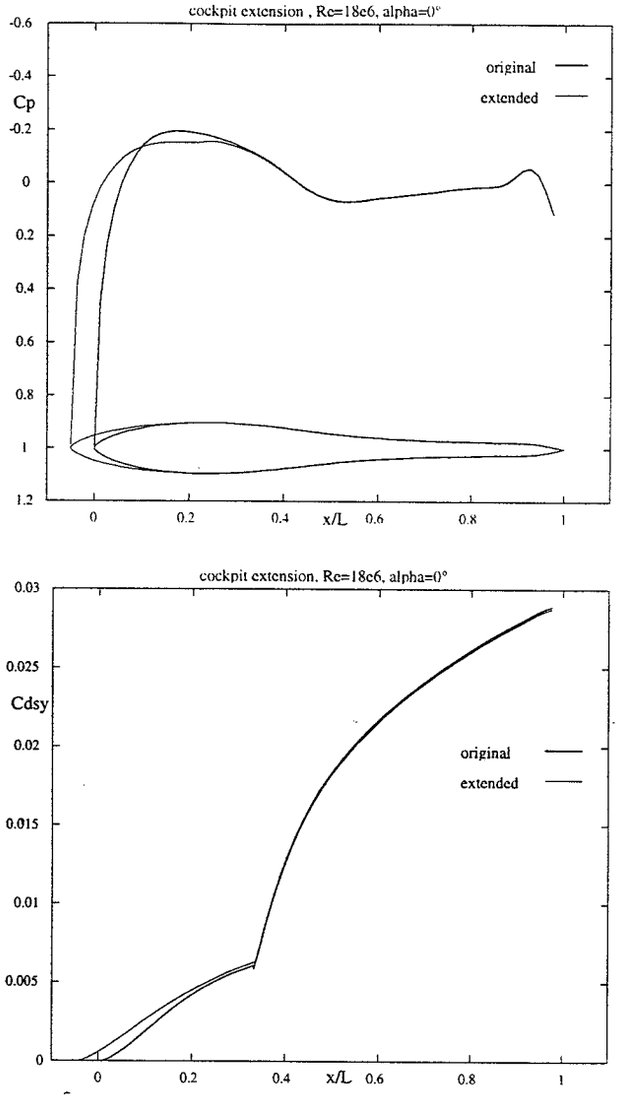

Figure 3: Effect of cockpit length increase.

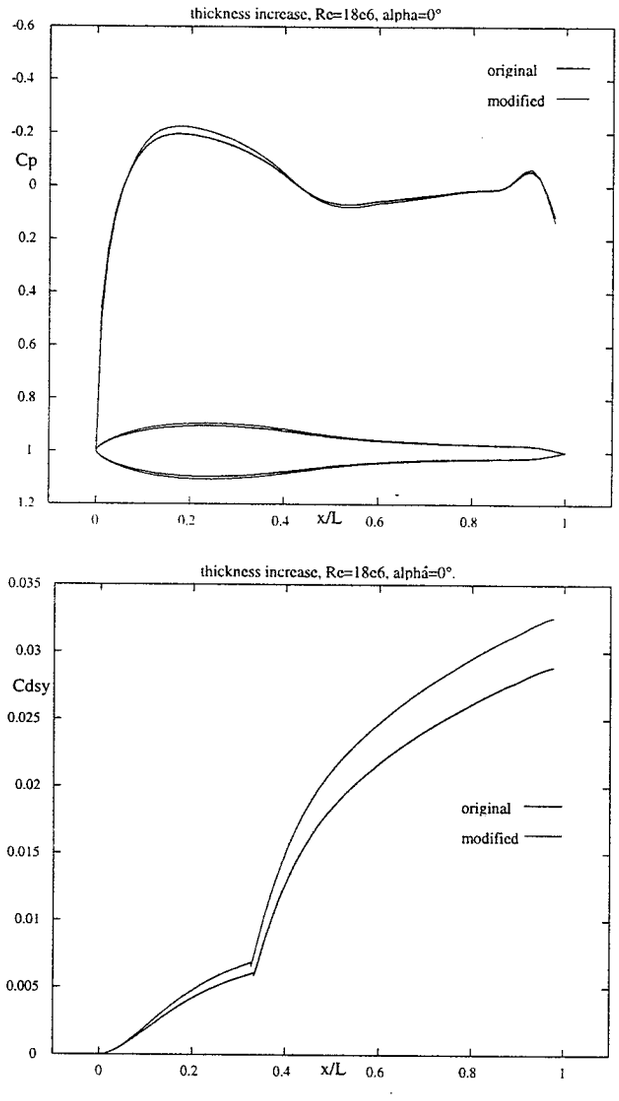

Figure 4: Effect of fuselage height increase.

Wing-fuselage interference effects

The interference effects of the flow on a high-performance sailplane wing-fuselage combination can be distinguished in non-viscous and viscous effects[4].

Non-viscous effects

Due to the displacement effect of the fuselage the streamwise pressure distribution on the wing changes towards the junction, depending on the relative dimensions and position of the fuselage and wing and resulting curvature of the intersection lines. As a result, the shape of the contraction, in particular the width contraction, will affect the pressures on the wing-root area.
Due to circulation the flow in front of and behind the wing is curved. To minimize drag, the fuselage shape of a high-performance sailplane is fitted to the streamlines of the wing at a certain lift coefficient (usually for the best glide ratio). At higher angles of attack there will be a crossflow and hence an upwash along the sides of the fuselage in front of the wing, named alpha-flow, which increases the angle of attack towards the wing root, see Figure 5a. At lower angles of attack there will be a downwash along the sides of the fuselage which decreases the angle of attack towards the wing root.

Viscous effects

The laminar boundary layer on the forebody of the fuselage is not able to overcome the adverse pressure gradient caused by the fuselage contraction and wing-root stagnation pressure, and turns turbulent, see Figure 5b. The turbulent boundary layer is not able to overcome the steep adverse pressure gradient in front of the wing-root

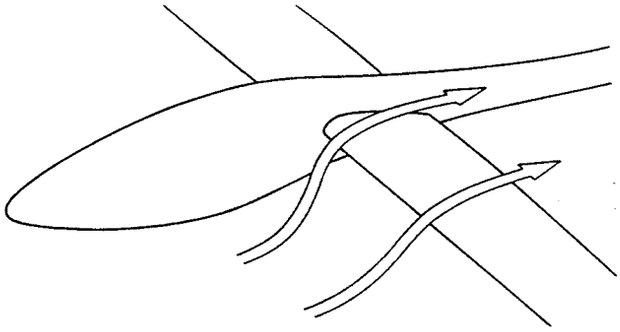

Figure 5a: Alpha-flow effect.

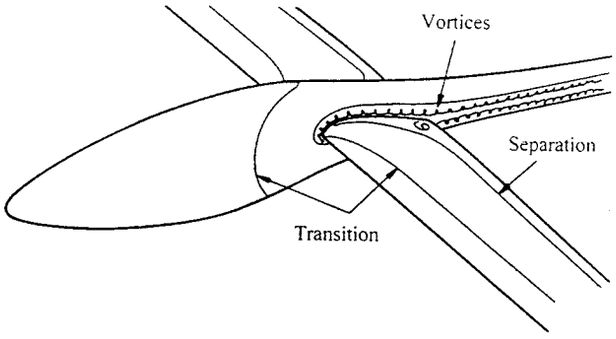

Figure 5b: Viscous flow effects.

leading edge either and separates from the surface along a separation line at some distance around the junction. The separated flow rolls up into a vortex system wrapped around the wing root, and on the wing root a turbulent wedge originates at the leading edge.
At the higher angles of attack, due to alpha-flow, the position of transition on the upper surface of the laminar wing shifts forward towards the wing root and turbulent separation will occur at the rear of the root region if the laminar wing airfoil is applied up to the fuselage, as shown in Figure 5b. On the lower wing surface, the position of transition shifts forward due to alpha-flow at the lower angles of attack.

Figure 6 shows flow patterns, visualized by fluorescent oil in U.V. light, on the upper and lower wing-fuselage surface of a high-performance sailplane windtunnel model. The curved transition lines due to the alpha-flow effect, and the separated flow on the wing-root upper surface are clearly visible. Zigzag tape, intended to trip the laminar boundary layer, is in the turbulent boundary layer now and produces small vortices.

Design objects and tools

In designing the wing-fuselage combinations described in the next sections, the interference effects were encountered by changing the laminar wing airfoil towards

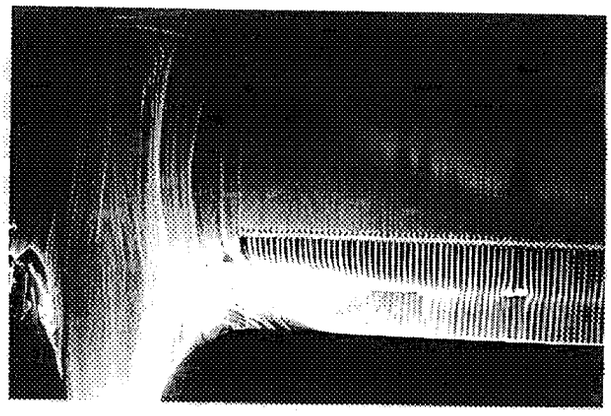

Figure 6a: Oil flow pattern on upper wing-fuselage surface.

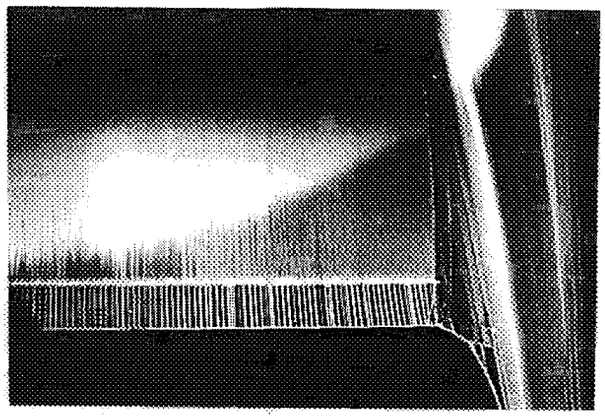

Figure 6b: Oil flow pattern on lower wing-fuselage surface.

the fuselage in order to preserve the laminar flow pressure distribution as far as possible up to the turbulent corner flow, where the target pressure distribution is suitable for the turbulent flow conditions. In the second design, the alpha-flow effect was encountered by cambering a shoulder wing in spanwise direction.
The laminar wing airfoils as well as the target pressure distributions for the turbulent wing-root section were designed with the two-dimensional airfoil analysis and design code XFOIL, developed by M. Drela[7]. The code is especially suitable for low-Reynolds-number airfoils where laminar separation bubbles play a detrimental role. It has a full-inverse design option, which permits the velocity distribution over the entire airfoil to be specified, as well as a mixed-inverse algorithm where the geometry is prescribed over a part of the airfoil surface and the velocity is prescribed over the remainder.
The wing-fuselage combinations were designed with the three-dimensional panel code KK-AERO, developed by K. Kubrynski[12]. The code has a design option as well, where differences between design and actual pressure

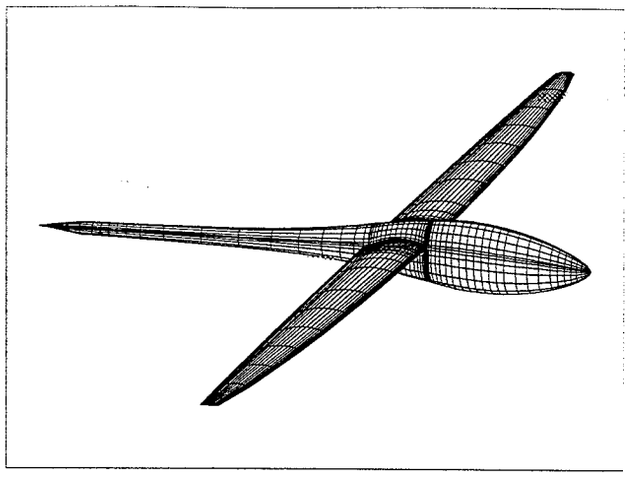

Figure 7: Initial wing-fuselage combination.

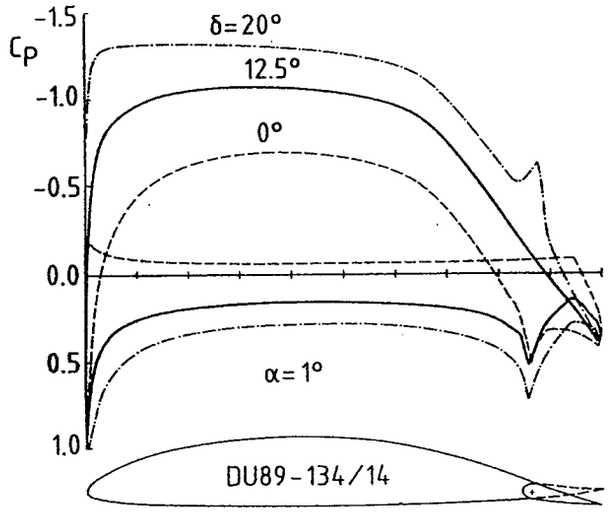

Figure 8: Potential flow pressure distributions on airfoil DU89-134/14.

distributions are minimized iteratively using a numerical optimization technique and taking geometrical constraints into account. The boundary layer on the wingstrips is calculated by the methods used in XFOIL, without viscous layer influence on the potential flow pressure distribution, however.

Design of a wing-fuselage combination with camber changing flap

Figure 7 shows the initial wing-fuselage combination with increased panel density at the junction. The wing with nearly elliptical chord distribution and straight flap hinge line, employs airfoil DU89-134/14 in the inner wing, Figure 8. This airfoil has a thickness of 13.4% chord and a camber changing flap of 14%, and was designed and windtunnel tested in the Low-Speed Low-Turbulence Windtunnel (LTT) of Delft University of Technology, Faculty of Aerospace Engineering[3]. A special feature is the low drag due to long laminar flow regions on the upper and lower surface, especially at the high speed zero degree flap deflection where the wing profile drag contributes about 55% to the total sailplane drag. A flexible slot sealing on the lower surface enables the boundary layer to remain laminar up to 95% chord, where blowing orifices cause transition, thus avoiding a detrimental laminar separation bubble. The hollow flap serves as the duct for the air supply to the blowing orifices, and the air enters the flap via a small inlet.

Figure 9 shows the operational conditions relevant for the wing-fuselage combination design, where (1), (2) and (3) are the high-, medium- and low-speed conditions respectively. Since the flight speed is primarily dictated by the flap deflection and the angle of attack hardly changes, the alpha-flow effect is mainly caused by the circulation generated by the flap deflection. The fuselage shape has been fitted to the streamlines of the wing at the lift coefficient for best glide ratio. The fuselage top-, bottom-

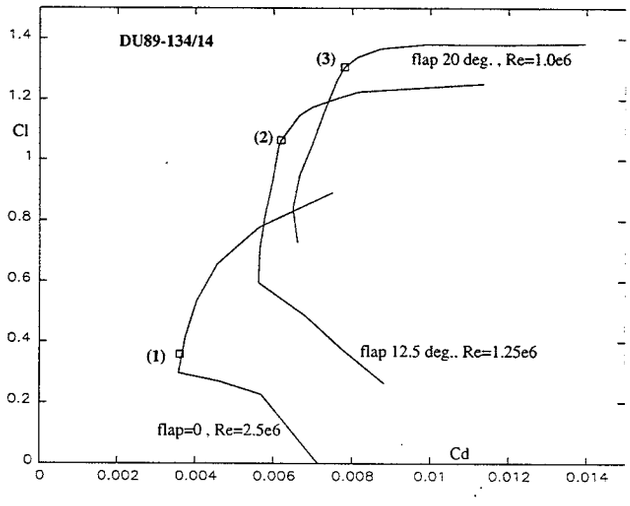

Figure 9: Operational conditions relevant for the junction design: 1) High speed, 2) Medium speed, 3) Low speed.

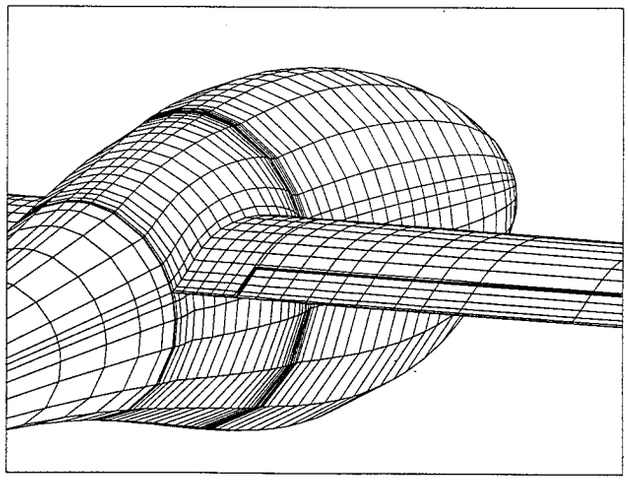

Figure 10: Initial configuration seen from behind.

and sideline are deduced from airfoil shapes, given the geometrical constraints of the cockpit size and the engine with retractable propeller behind the cockpit. The contraction of the fuselage width in the wing-root region was carefully shaped in view of the displacement effect on the wing. The cross sections of the fuselage are defined by deformed ellipses with continuous curvature along the circumference.

Figure 10 shows the initial configuration seen from behind. The flap is set at the medium speed 12.5 degrees deflection, where the upper surface is smooth without a kink at the hinge position. (The lower surface is smooth at the high-speed zero-degree flap deflection). Figure 11 shows two-dimensional airfoil pressure distributions: at a lift coefficient of 1.0 with transition free (Figure 11a), and at the same angle of attack with transition fixed on the nose (Figure 11b). The dotted line is the non-viscous pressure distribution. The flat pressure distribution on the flap in the latter case, due to separated flow, illustrates that this pressure distribution is not suitable for the turbulent junction flow. Hence, the upper surface was modified; Figure 11c shows the resulting pressure distribution with full turbulent flow and no separation. The dotted non-viscous pressure distribution was used as target for the root of the wing-fuselage design.

The pressure distribution on the wing-root area of the initial wing-fuselage combination, Figure 12, shows suction peaks on the leading edge due to displacement and alpha-flow effects. During the design iterations with the KK-AERO code, attempting to realize the target pressure distributions in the region between the fuselage and the flap, it turned out that the new wing upper surface near the fuselage at 60% chord would be thinner than the initial shape. This undesirable sag in the wing-root region was eliminated by extending the chord at the wing root, thus creating a trailing edge fairing. It also became clear that the target pressure level at the wing root, especially at the leading edge, would lead to an unrealistic shape. The target pressure distribution was adjusted by keeping the same adverse pressure gradient but at a higher pressure level. The resulting shape and pressure distributions are shown in Figure 13. The cross sections in the region between the fuselage and the flap are shown in Figure 14; the thickness is blown up for the sake of clarity. This figure also shows the changes on the lower surface, designed with the flap at the high-speed zero-degree deflection. Due to a careful design of the fuselage-width contraction, a suction peak on the leading edge of the lower-wing surface could be avoided. The lower-surface thickness could be increased and the kink at the hinge position removed, thus creating space for the automatic connections of the steering rods. Laminar flow on the lower surface of the wing up to 95% of the chord could be preserved nearly up to the turbulent corner wedge, see Figure 15. On the upper surface the transition line is straight almost up to the turbulent corner wedge at the medium and low-speed flap deflections, as shown in Figure 16. As mentioned before, the boundary layer calculations in KK-AERO are performed for the potential flow pressure distribution and the effect of the boundary layer on the pressure distribution is not taken into account. Consequently, the separation location, shown in Figure 16, is predicted too early. The XFOIL results in Figure 11 showed that separation will not take place.

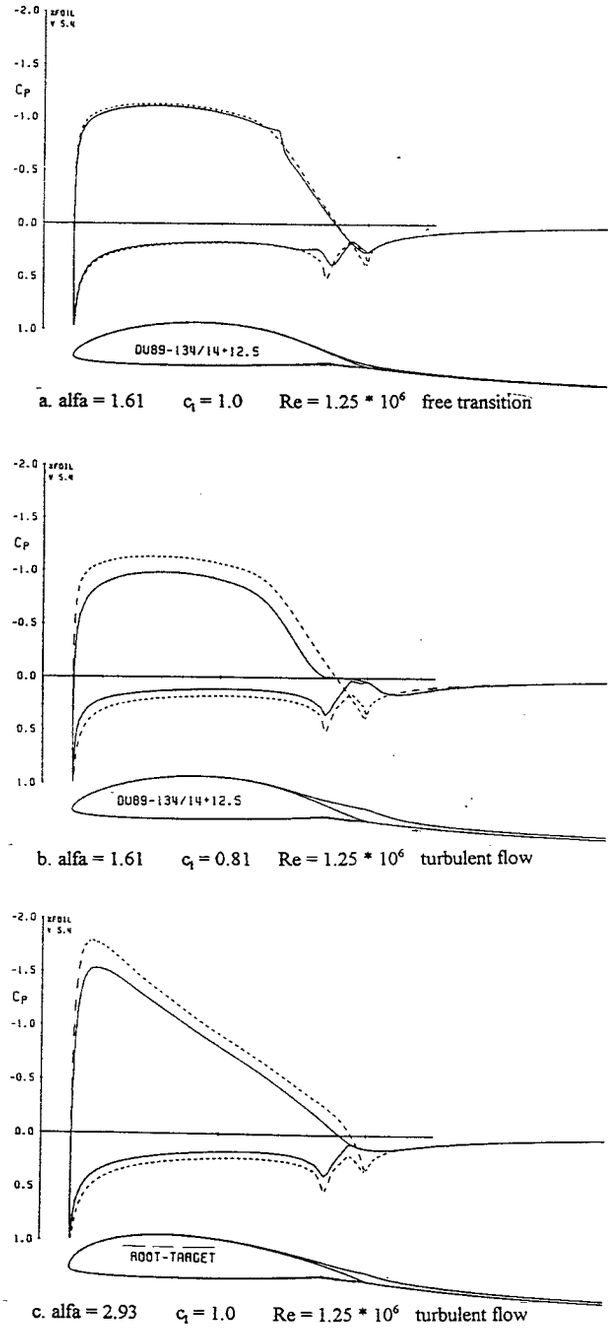

a. alfa = 1.61 c_l = 1.0 Re = 1.25 * 10^6 free transition

b. alfa = 1.61 c_l = 0.81 Re = 1.25 * 10^6 turbulent flow

c. alfa = 2.93 c_l = 1.0 Re = 1.25 * 10^6 turbulent flow

Figure 11: Two-dimensional airfoil pressure distributions.

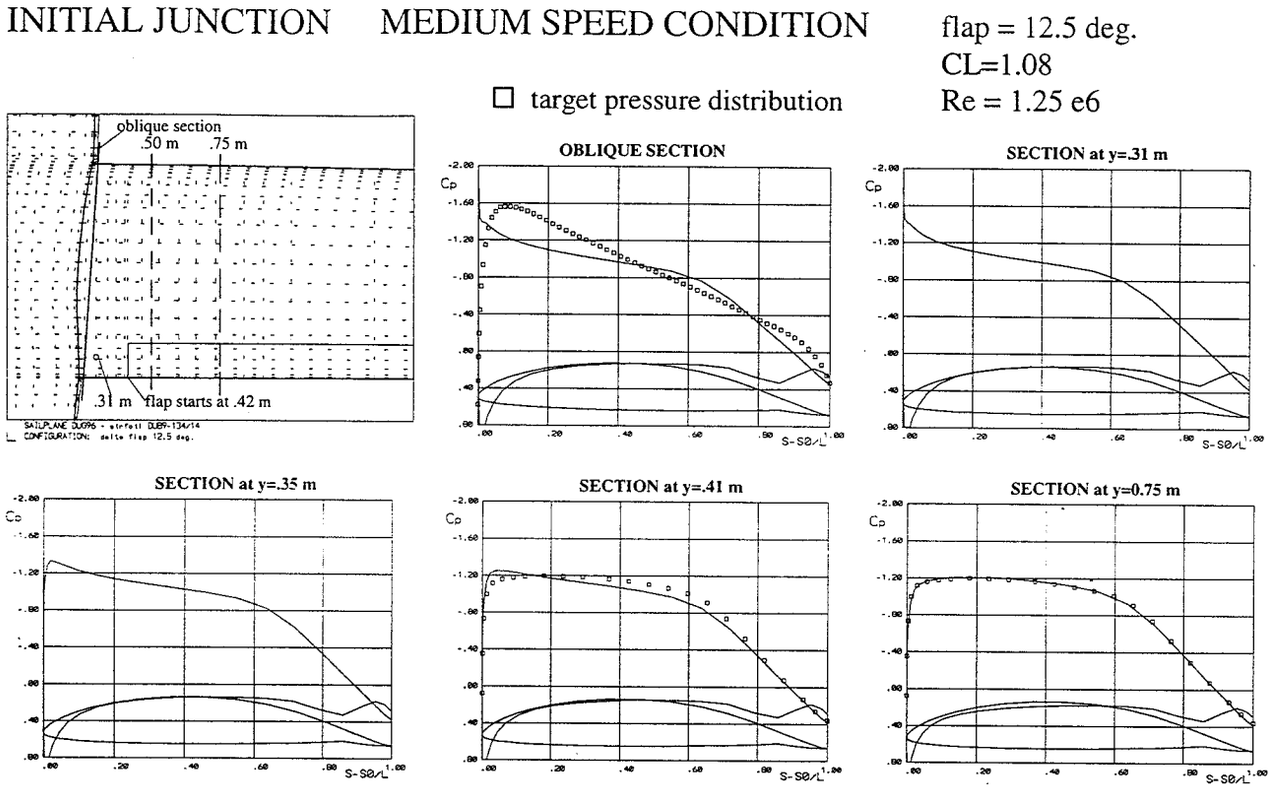

Figure 12: Pressure distributions on initial configuration.

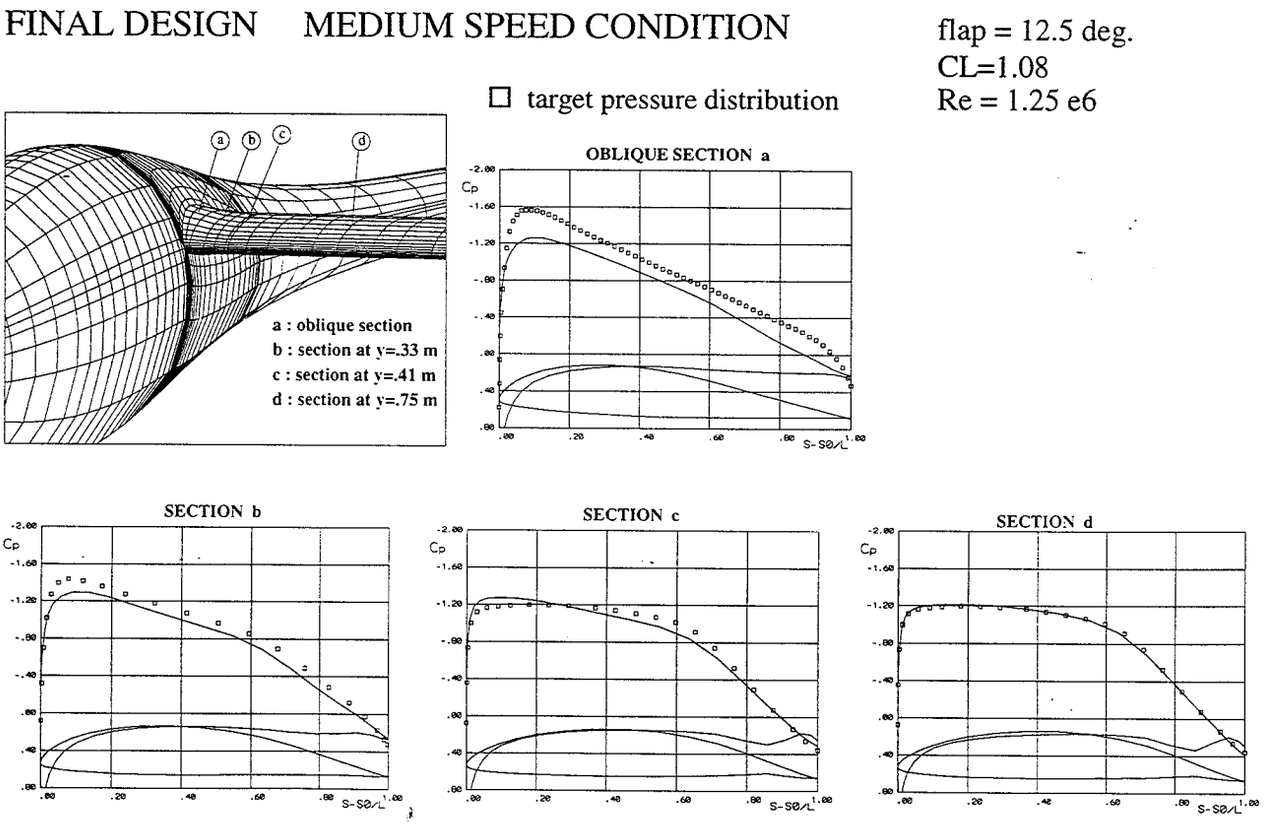

Figure 13: Pressure distributions on final design.

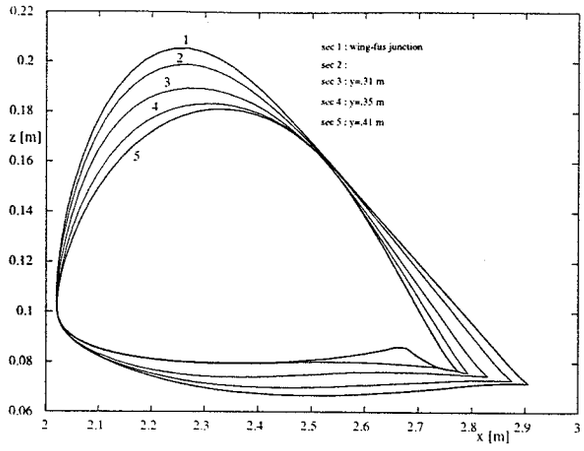

Figure 14: Cross sections between fuselage and flap.

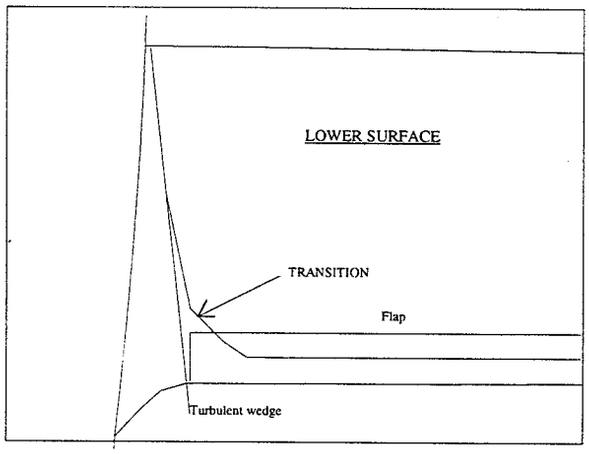

Figure 15: Transition position on lower surface wing design at high speed condition.

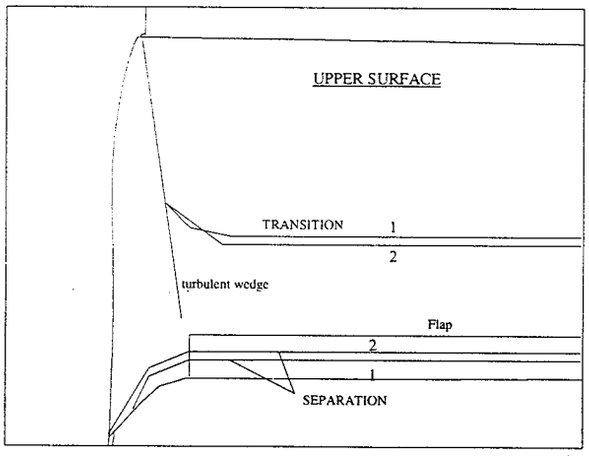

Figure 16: Transition and separation on upper surface wing design at medium-speed (2) and low-speed (1) condition.

Design of a wing-fuselage combination with spanwise camber

The wing of a Standard Class sailplane has no flap. The flight speed depends on the angle of attack and due to the rotation of the fuselage the alpha-flow effect is larger than in the previous case. This effect can be encountered by cambering the wing in spanwise direction[14], as will be shown.

Consider a circular cylinder with infinite length at an angle of attack. According to the independence principle of Busemann[13] the longitudinal and transverse velocity components of the approaching flow can be considered separately. While the longitudinal velocity component is constant everywhere in the flow field, the transverse component changes depending on the position. This component is for instance zero at the bottom and top of the cylinder, and doubled at the side. As a consequence, the flow angle is zero at the top and bottom of the cylinder and doubled at the side. Figure 17 shows the change of the flow angle along some equipotential lines (lines perpendicular to the streamlines of the transverse flow) which start at some point at θ on the cylinder. The flow angle changes only a few percent along the line starting at $\theta = 30°$.

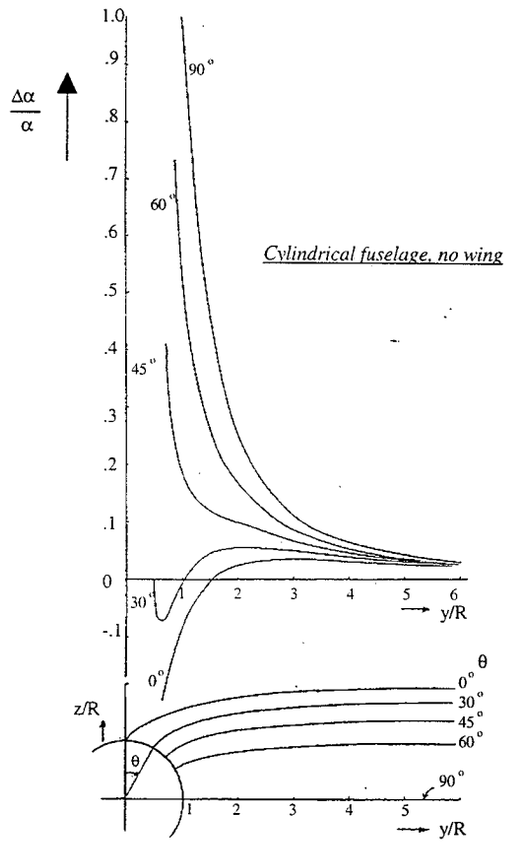

Figure 17: Flow angle along equipotential lines; cylindrical fuselage, no wing.

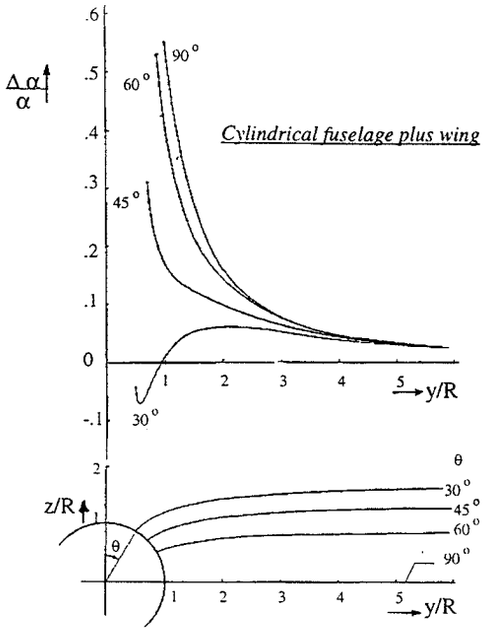

Figure 18: Flow angle at leading edge of wings cambered along equipotential lines, cylindrical fuselage.

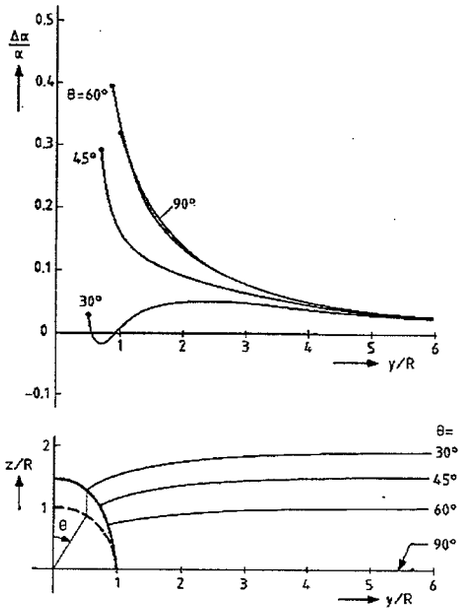

Figure 19: As figure 18, fuselage with elliptical cross section.

When a wing is added to the cylinder the flow direction is affected, depending on the position of the wing. For instance, in case of a midwing the flow at the wing is directed parallel to the cylinder axis and the angle of the flow approaching the leading edge is reduced with respect to the no-wing case. Figure 18 shows the results for wings cambered along an equipotential line; again, the flow angle changes only a few percent for a cambered wing starting at $\theta = 30°$. High-performance sailplane fuselages have nearly elliptical cross sections. A corresponding transformation of the flow system leads tot the results presented in Figure 19. While the flow angle at the wing-root leading edge of a midwing is still increased by about 33%, the angle changes only a few percent in case of a shoulder wing cambered along an equipotential line starting at $\theta = 30°$. These findings were used in designing the wing-fuselage combination of a Standard Class sailplane with cambered shoulder wing. The core of the fuselage, needed to produce the mould, already existed but was modified in the contraction region to match with the cambered wing.

The effects of viscosity were encountered in the same way as in the previous design case. Figure 20a shows potential flow pressure distributions at high-speed and low-speed conditions of the laminar wing airfoil DU91-122, designed and windtunnel tested in the LTT. This airfoil has laminar flow up to 95% of the chord on the lower surface too, but now a zigzag tape turbulator is the proper device to trip the boundary layer. The upper surface pressure distribution was modified to be suitable for the turbulent flow at the wing root, Figure 20b. According to the predictions of XFOIL the flow on the upper surface of

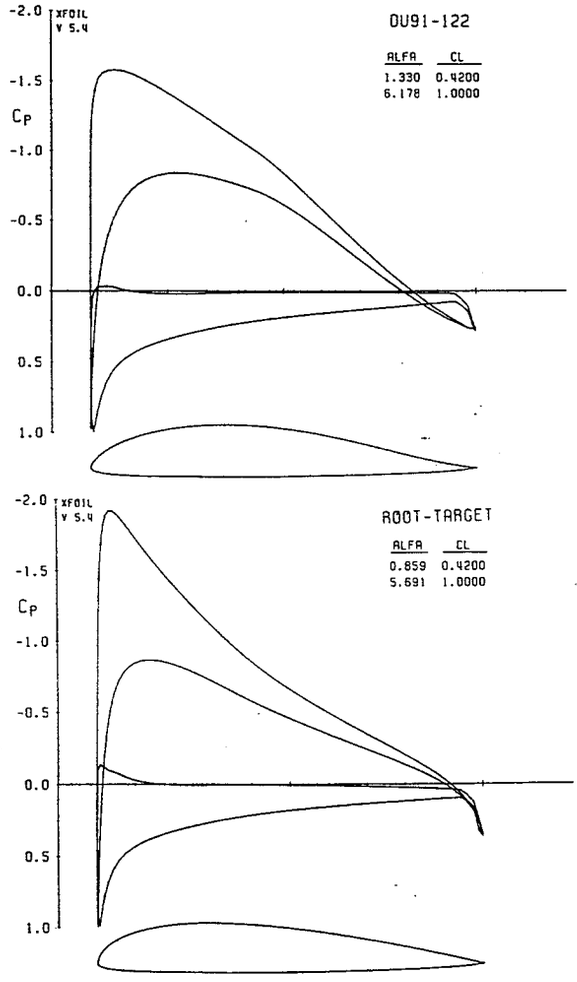

Figure 20: Two-dimensional potential flow pressure distributions: a) airfoil DU91-122 and b) target upper surface pressure distribution.

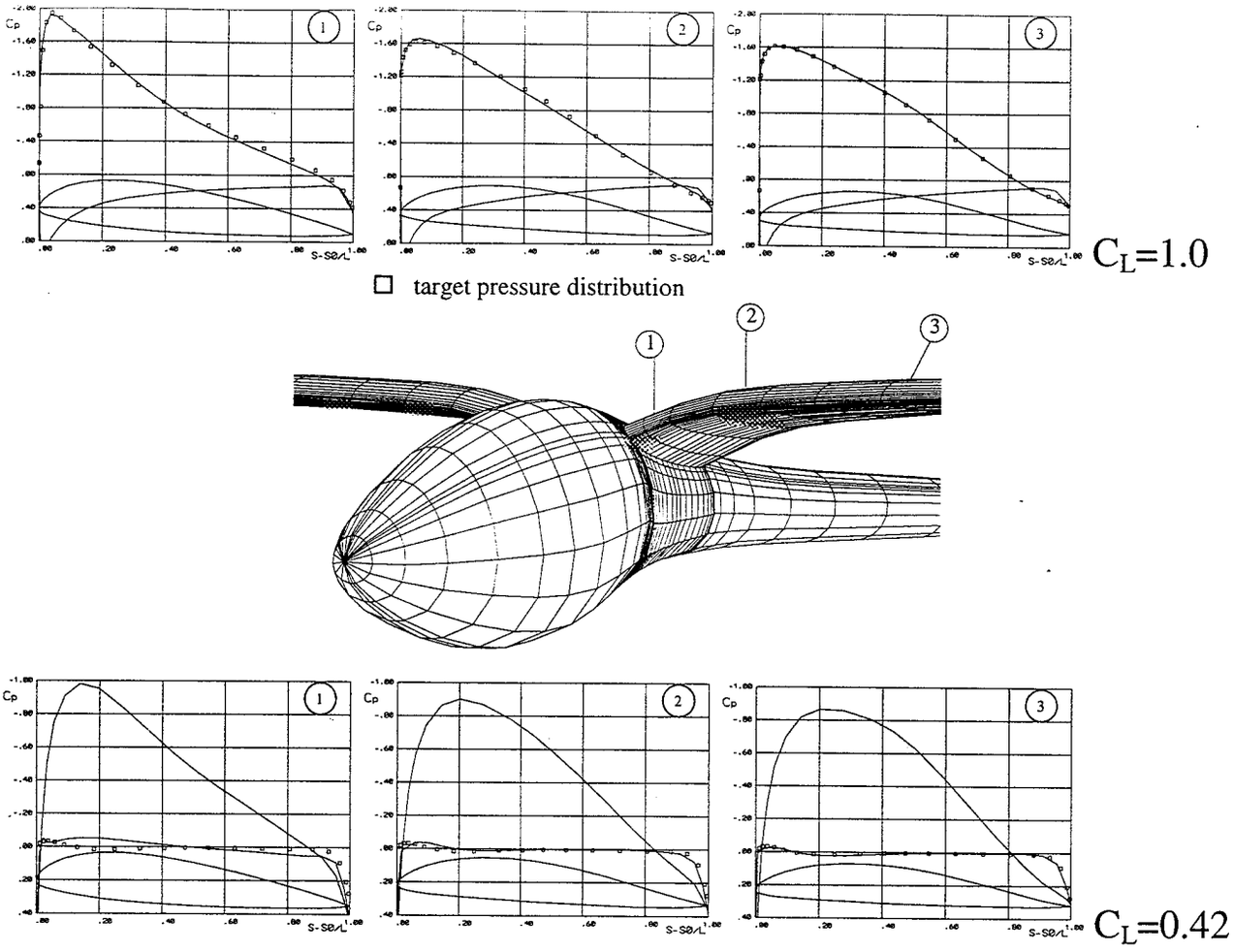

Figure 21: Target and actual pressure distributions on wing-fuselage design with spanwise cambered wing.

the laminar wing airfoil with transition free, and on the modified airfoil with transition fixed on the nose, starts to separate at a lift coefficient of 1.3.

Figure 21 presents the target and actual pressure distributions as designed with the KK-AERO code. The change in airfoil shape towards the wing root is clearly shown. The design of this configuration with prescribed spanwise camber was relatively easy due to the absence of the alpha-flow effect.

Figure 22 shows the calculated position of transition on the upper and lower wing surface. In comparison with a planar midwing configuration with laminar airfoil DU91-122 up to the fuselage (not shown here), the spanwise cambered design has the same chordwise transition position on the upper surface, but turbulent separation in the root region is eliminated and transition on the lower surface of the cambered wing occurs substantially more backwards.

Concluding remarks

Numerically milled scale 1:3 windtunnel models have been produced of the fuselage and center section of the spanwise cambered wing and planar midwing mentioned before. Oil-flow patterns substantiated the calculated transition and separation results. However, due to an improper lofting procedure the leading edge of the cambered wing, at a location next to the straight part, was too sharp, causing locally earlier transition and separation on the upper surface at higher angles of attack, and earlier transition on the lower surface at lower angles of attack. Although the benefits in performance could not be proven by windtunnel tests yet, prototypes of both the wing-fuselage design with camber changing flap and with spanwise camber are being produced in Germany.

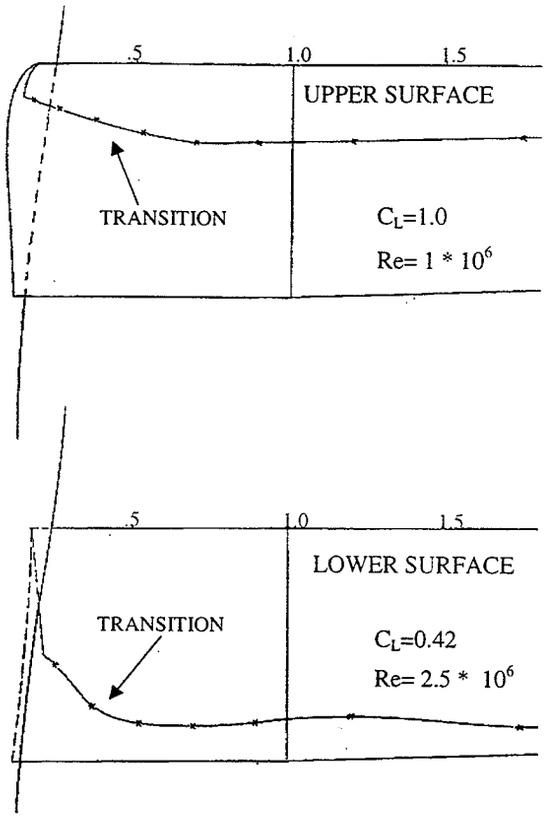

Figure 22: Transition position on upper and lower surface of spanwise cambered wing design.

References

1. Boermans, L.M.M. and Selen, H.J.W.: Design and tests of airfoils for sailplanes with an application to the ASW-19B. ICAS-82-5.5.2, 1982.

2. Boermans, L.M.M. and Waibel, G.: Aerodynamic and structural design of the Standard Class Sailplane ASW-24. ICAS-88-2.7.7,1988.

3. Boermans, L.M.M. and Garrel, A. van: Design and windtunnel test results of a flapped laminar flow airfoil for high-performance sailplane applications. ICAS-94-5.4.3, 1994.

4. Boermans, L.M.M. and Terleth, D.C.: Windtunnel tests of eight sailplane wing-fuselage combinations. Technical Soaring 8, No. 3, 1984.

5. Devenport, W.J. and Simpson, R.L.: Flow past a wing-body junction – Experimental evaluation of turbulence models. AIAA J. 30, p. 873-881, 1992.

6. Coiro, D.P. and Nicolosi, F.: Design of Natural Laminar Flow Fuselages. ICAS-94-4.7.4, 1994.

7. Drela, M.: XFOIL, an analysis and design system for low Reynolds number airfoils. Low-Reynolds-number aerodynamics, Ed. T.J. Mueller, Lecture Notes, 1989.

8. Young, A.D.: The calculation of total and skin friction drag of bodies of revolution at zero incidence. ARC R&M 1874, 1939.

9. Althaus, D.: Windtunnel measurements on bodies and wing-body combinations. Motorless Flight Research, NASA CR-2315, 1972.

10. Sperber, M.: Untersuchung des Insassenschutzes bei Unfällen mit Segelflugzeugen und Motorseglern. TÜV Rheinland Kraftfahrt GmbH, L-2/93-50112/92, 1998.

11. Sperber, M.: Gesamtrückhaltesysteme in Segelflugzeugen. TÜV Rheinland Kraftfahrt GmbH, L-1/90-9050090/90, 1992.

12. Kubrynski, K.: Design of 3-dimensional complex airplane configurations with specified pressure distribution via optimization. Proceedings of ICIDES III Conference, Ed. G.S. Dulikravich, Washington D.C., 1991.

13. Jones, R.T.: Wing Theory. Princeton University Press, Princeton, New Yersey, p. 91, 1990.

14. Boermans, L.M.M., Kubrynski, K. and Nicolosi, F.: Wing-fuselage design of high-performance sailplanes. In: Boundary-Layer Separation in Aircraft Aerodynamics. Delft University Press, 1997.